

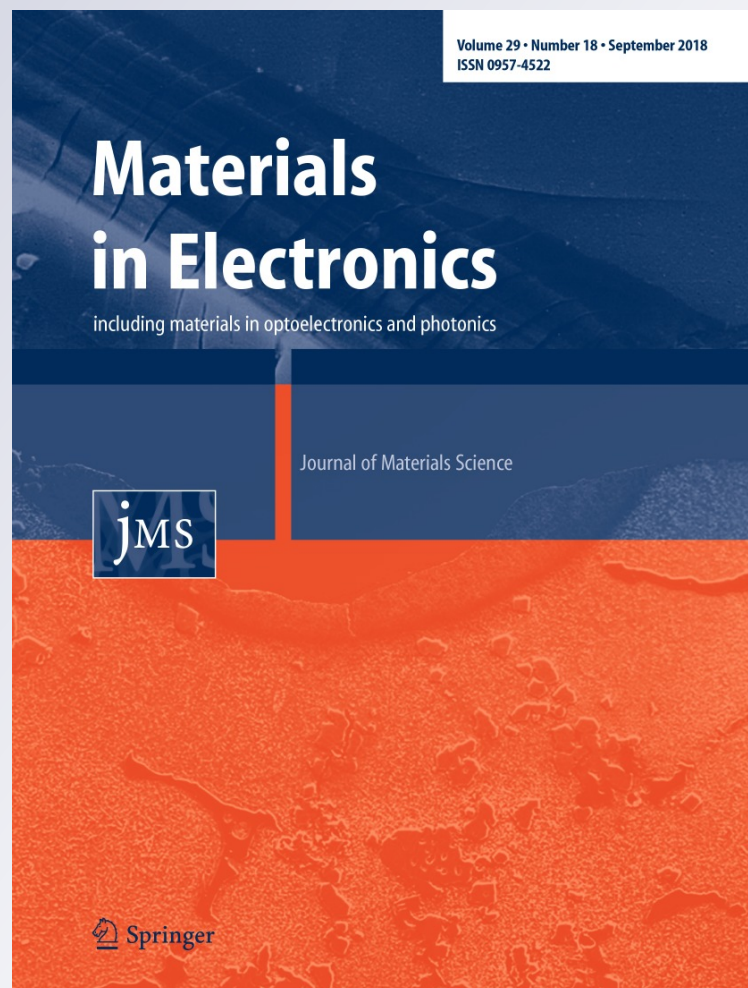
Electronic band-structure and optical constants of Pb₂GeS₄: Ab initio calculations and X-ray spectroscopy experiments

**Tuan V. Vu, A. A. Lavrentyev,
B. V. Gabrelian, L. N. Ananchenko,
O. V. Parasyuk, Olha Karaim &
O. Y. Khyzhun**

**Journal of Materials Science:
Materials in Electronics**

ISSN 0957-4522
Volume 29
Number 18

J Mater Sci: Mater Electron (2018)
29:16088-16100
DOI 10.1007/s10854-018-9698-4



Your article is protected by copyright and all rights are held exclusively by Springer Science+Business Media, LLC, part of Springer Nature. This e-offprint is for personal use only and shall not be self-archived in electronic repositories. If you wish to self-archive your article, please use the accepted manuscript version for posting on your own website. You may further deposit the accepted manuscript version in any repository, provided it is only made publicly available 12 months after official publication or later and provided acknowledgement is given to the original source of publication and a link is inserted to the published article on Springer's website. The link must be accompanied by the following text: "The final publication is available at link.springer.com".



Electronic band-structure and optical constants of Pb_2GeS_4 : *Ab initio* calculations and X-ray spectroscopy experiments

Tuan V. Vu^{1,2} · A. A. Lavrentyev³ · B. V. Gabrelian⁴ · L. N. Ananchenko³ · O. V. Parasyuk⁵ · Olha Karaim⁶ · O. Y. Khyzhun⁷Received: 16 June 2018 / Accepted: 18 July 2018 / Published online: 21 July 2018
© Springer Science+Business Media, LLC, part of Springer Nature 2018

Abstract

The electronic band-structure of the ternary sulfide Pb_2GeS_4 was investigated by combining experimental and theoretical methods. Binding energy (BE) values of core electrons of Pb_2GeS_4 are measured employing X-ray photoelectron spectroscopy (XPS) for as-synthesized and treated with Ar^+ -ions crystal surfaces. The XPS measurements indicate that Ar^+ -ion treatment does not change the BE values of the core-level electrons of atoms constituting the Pb_2GeS_4 single crystal as well as peculiarities of the XPS valence band (VB) spectrum. The treatment does not cause changes in the crystal surface stoichiometry. The band-structure calculations based on density functional theory (DFT) reveal total density of states and partial densities of states of Pb_2GeS_4 within different exchange–correlation approximations. The best fit with the experiment is derived when the DFT calculations of Pb_2GeS_4 employ modified Becke–Johnson potential with Hubbard-corrected functional and taking into account spin–orbit (SO) interaction. The calculations indicate that top and upper portion of the VB is composed mainly by S 3p states, its central portion is formed by Ge 4p and S 3p states, while contributions of Pb 6s states dominate at its bottom with slightly smaller contributions of Ge 4s states as well. Contributions of unoccupied Pb 6p states dominate at the conduction band (CB) bottom. Regarding the occupation of the VB by Ge 4p and S 3p states, the theoretical data are confirmed experimentally by matching the XPS VB spectrum on a common energy scale with the X-ray emission spectra representing the valence S p and Ge p states. The present calculations yield that the VB maximum is positioned at the Y point, while the CB minimum at the Γ point; this fact indicates that Pb_2GeS_4 sulfide is an indirect-gap material. The principal optical constants are also elucidated using the *ab initio* DFT calculations.

✉ O. Y. Khyzhun
khyzhun@ukr.net; khyzhun@ipms.kiev.ua

Tuan V. Vu
vuvantuan@tdt.edu.vn

A. A. Lavrentyev
alavrentyev@dstu.edu.ru

B. V. Gabrelian
boris.gabrelian@gmail.com

O. V. Parasyuk
Parasyuk.Oleg@eenu.edu.ua

Olha Karaim
olgakaraim@ukr.net

¹ Division of Computational Physics, Institute for Computational Science, Ton Duc Thang University, Ho Chi Minh City, Vietnam

² Faculty of Electrical & Electronics Engineering, Ton Duc Thang University, Ho Chi Minh City, Vietnam

³ Department of Electrical Engineering and Electronics, Don State Technical University, 1 Gagarin Square, Rostov-on-Don, Russian Federation 344010

⁴ Department of Computational Technique and Automated System Software, Don State Technical University, 1 Gagarin Square, Rostov-on-Don, Russian Federation 344010

⁵ Department of Inorganic and Physical Chemistry, Lesya Ukrainka Eastern European National University, 13 Voli Avenue, Lutsk 43025, Ukraine

⁶ Department of Ecology and Environmental Protection, Lesya Ukrainka Eastern European National University, 13 Voli Avenue, Lutsk 43025, Ukraine

⁷ Frantsevych Institute for Problems of Materials Science, National Academy of Sciences of Ukraine, 3 Krzhynivsky Street, Kyiv 03142, Ukraine

1 Introduction

Interaction of germanium and lead, the IV group elements of the Periodic Table, with sulfur and selenium causing the formation of binary compounds yields different cation valences, namely II or IV, in the case of monochalcogenides and dichalcogenides [1, 2]. The interaction of the monochalcogenides and dichalcogenides having octahedral and tetrahedral cation coordinations produces the formation of ternary chalcogenides, which reveal mixed cation coordination [2]. In accordance with the equilibrium phase diagram of the PbS–GeS₂ system [3], two ternary sulfides, namely Pb₂GeS₄ and PbGeS₃, with crystal structure belonging to monoclinic space group (SG) P2₁/c, are known to exist [4, 5]. Both ternary sulfides are high-resistance semiconductors revealing substantial photosensitivity even without additional thermal treatment and any special activation [6]. Raman spectra of PbGeS₃ and Pb₂GeS₄ crystals were studied in detail in Refs [7, 8], to explore vibration modes in these compounds. In particular, considerable splitting of the vibration modes in the Pb₂GeS₄ crystal was established to be associated with strong deformation of [GeS₄]⁴⁻ anions by the crystal field, whereas the relative intensities of the ν_1 and ν_3 modes were found to be comparable in this crystal that prevent their identification.

Crystal structure of Pb₂GeS₄ is presented in Fig. 1. In this structure, there exist two and four non-equivalent Wyckoff positions for lead and sulfur atoms, respectively (Table 1) and the structure is layered (Fig. 2a). It can be viewed as formed by isolated [GeS₄] tetrahedra and Pb²⁺ ions (Fig. 2b). The [GeS₄] tetrahedron is almost undistorted, while the [Pb₍₁₎S₇] and [Pb₍₂₎S₇] polyhedra reveal their substantial distortion (Fig. 3). The unit-cell dimensions of Pb₂GeS₄ compound were determined as follows: $a = 7.9742(6)$ Å, $b = 8.9255(8)$ Å, $c = 10.8761(8)$ Å, $\beta = 114.171(9)^\circ$, $Z = 4$ [4]. This low-temperature structure is stable up to temperature of 610 ± 10 °C, and, at

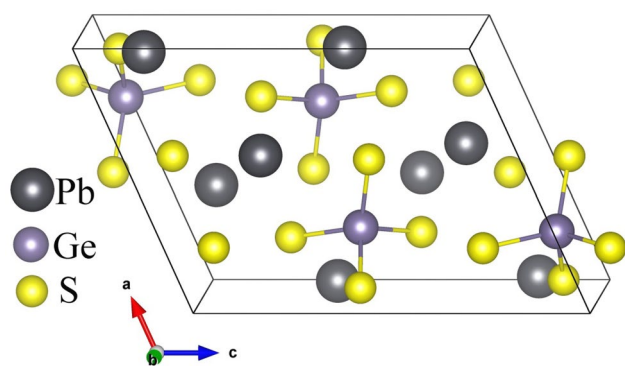


Fig. 1 Crystal structure of Pb₂GeS₄ compound

Table 1 Atomic positions (x , y , and z) used in the present band-structure calculations of Pb₂GeS₄ (space group P2₁/c, $a = 7.9742$ Å, $b = 8.9255$ Å, $c = 10.8761$ Å, $\beta = 114.171^\circ$ [4])

Atom	x	y	z
Pb1	0.0356	0.3161	0.3407
Pb2	0.4124	0.4326	0.1551
Ge	0.7137	0.1908	0.0063
S1	0.2465	-0.0171	0.1256
S2	0.7644	0.0900	0.2027
S3	0.4437	0.2002	0.3980
S4	0.9193	0.3691	0.0610

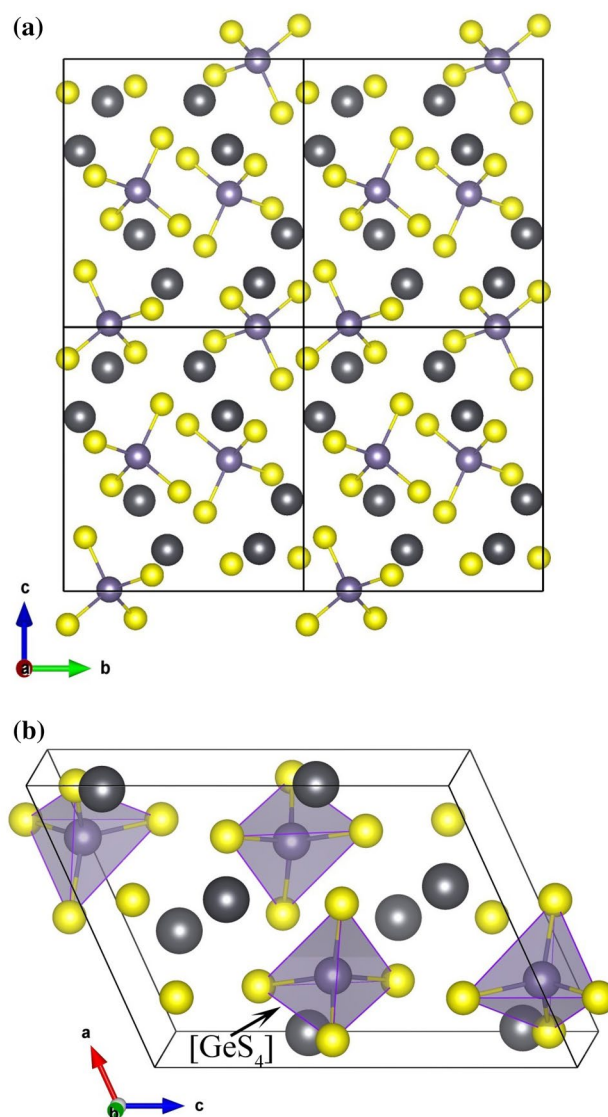


Fig. 2 **a** Structure of the layers viewed down the a -axis and **b** the staking of [GeS₄] tetrahedra in Pb₂GeS₄ compound

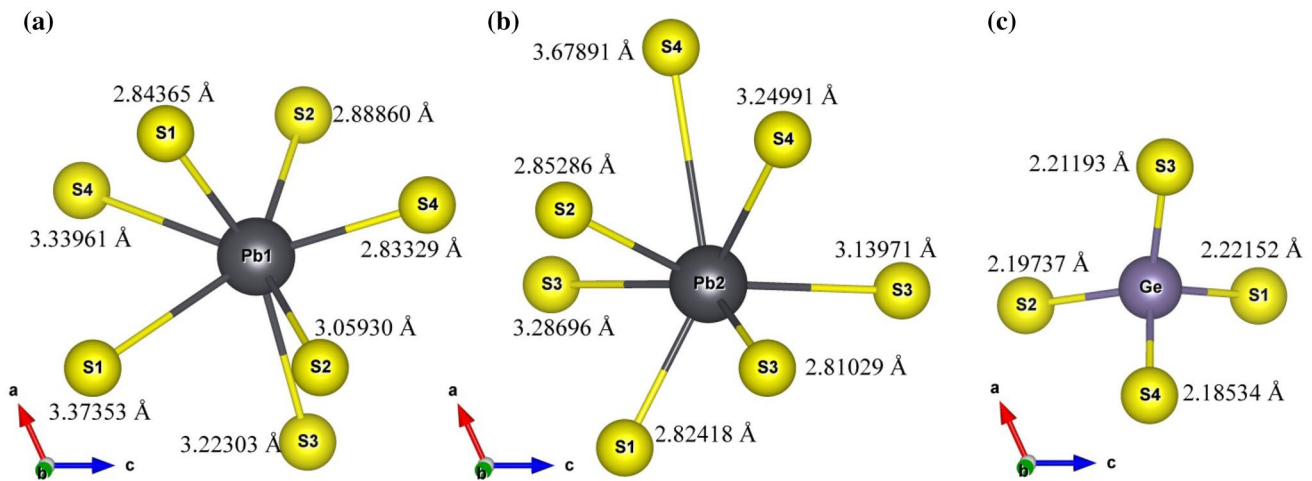


Fig. 3 The neighbor surroundings of **a** Pb1, **b** Pb2 and **c** Ge atoms within $[\text{PbS}_7]$ polyhedra and $[\text{GeS}_4]$ tetrahedra in the Pb_2GeS_4 structure

higher temperatures, monoclinic Pb_2GeS_4 sulfide reveals the polymorphic transition to a cubic $\alpha\text{-Pb}_2\text{GeS}_4$ phase (SG $\bar{1}43d$, $Z = 16$) with the lattice parameter $a = 14.096(4)$ Å [9]. This structure was established to be stable when substituting lead for tin and sulfur for selenium in a wide-range $\text{Pb}_{2-x}\text{Sn}_x\text{GeS}_{4-y}\text{Se}_y$ solid solution, with $0 \leq x \leq 0.5$ and $0 \leq y \leq 4$ [9]. The transition of monoclinic Pb_2GeS_4 to its cubic $\alpha\text{-Pb}_2\text{GeS}_4$ polymorph is well identified by changing color from orange to red [9–11]. Measurements of temperature dependence of dark electrical conductivity indicate that activation energy of monoclinic Pb_2GeS_4 sulfide is equal to 1.2 eV [6], while studies of the optical absorption edges reveal that the band gap energy, E_g , of Pb_2GeS_4 is equal to 2.29 ± 0.01 at room temperature [6].

It is worth mentioning that the electronic band-structure of solids is one of the key characteristics determining their physical and chemical properties and its knowledge gives possibilities for prediction of changing and tuning these properties to the desirable technological values [12, 13]. To the best of our knowledge, the electronic band-structure of Pb_2GeS_4 has not been investigated yet. To fill this lack, in the present work we carry out a complex study of the electronic band-structure of Pb_2GeS_4 involving both experimental and theoretical techniques. In particular, we perform first principles band-structure calculations, which are based on density functional theory (DFT), to elucidate features of total density of states (DOS) and partial DOS (PDOS) of Pb_2GeS_4 . Furthermore, to verify data of our calculations, we also use basic experimental methods, which probe total DOS and PDOS of solids, namely X-ray photoelectron spectroscopy (XPS) and X-ray emission spectroscopy (XES) to measure available informative spectra of Pb_2GeS_4 single crystal. In addition, the basic optical constants of the compound under study are elucidated by the present DFT calculations.

2 Experimental

2.1 Single crystal growth of Pb_2GeS_4

The Pb_2GeS_4 crystal was grown using Bridgman–Stockbarger method. The synthesis and growth were combined in the same quartz container with a conical bottom. Pb_2GeS_4 was synthesized from high-purity elements, namely Pb (99.99 wt.%), Ge (99.9999 wt.%), S (99.999 wt.%). However, Pb was additionally purified by dripping its melt through crushed quartz under dynamic vacuum. The evacuated and soldered ampoule was first heated in oxygen-gas burner flame to complete bonding of elementary sulfur. Then, the ampoule was placed in a shaft-type furnace and heated to 1070 K at the rate of 40 K/hr. The ampoule was kept at this temperature for 10–12 h with periodic vibration and cooled with the furnace turned off. The ampoule was then shortened to minimize free volume above the melt and transferred to the pre-heated two-zone vertical growth furnace. The temperature in the growth zone (upper zone) was 1040, and 720 K in the annealing zone (bottom zone). The temperature gradient at the solid-melt interface was thus 3.5 K/mm. After melting the batch the ampoule was shifted to lower temperatures crystallizing 5 mm of the melt and holding recrystallization annealing for 100 h. Then 2–3 mm of the seed was melted, and the crystal was grown onto the seed by lowering the growth container along the steady temperature profile of the furnace. The growth rate employed was 5 mm/day. After completing the crystallization, the ampoule with the crystal was transferred to the isothermal section of the annealing zone where it was kept for 200 h. Then both zones were synchronously cooled to room temperature at the rate of 120 K/day. The as-obtained Pb_2GeS_4 boule is shown in Fig. 4.



Fig. 4 Grown boule of Pb_2GeS_4 (illuminated from below with white light)

2.2 XPS and XES measurements

Experimental studies of the electronic structure of the Pb_2GeS_4 crystal employed the principal X-ray spectroscopy techniques that are generally used for such goal, namely XPS and XES. The present X-ray spectroscopy measurements deal with the Pb_2GeS_4 crystal shaped as a comparatively thin plate with the dimensions $8.5 \times 6.4 \times 1.1 \text{ mm}^3$. The XPS experiments were performed in an ion-pumped chamber under residual pressure less than 8.5×10^{-10} mbar using the UHV-analysis-system (SPECS Surface Nano Analysis Company, Berlin, Germany) operated by a Mg $K\alpha$ source ($E = 1253.6 \text{ eV}$). The XPS spectra were acquired at constant pass energy of 30 eV. The spectrometer energy scale was calibrated as reported elsewhere [14] and the charging effects were accounted for in the reference to the carbon 1s line [adventitious carbon, binding energy (BE) of 284.6 eV] as it is recommended for such kind of ternary Pb- and/or Ge-containing sulfides [15–17]. However, taking into account the fact that, when exciting the XPS spectra with a Mg $K\alpha$ source, the C 1s core-level spectrum superimposes the Auger Ge $L_2M_{23}M_{23}$ line in the Pb_2GeS_4 crystal, we also verified the charging effect by recording the core-level spectra with application of a flood gun as it is suggested for such a case [18]. To remove surface impurities and to check crystal stability regarding Ar^+ -ion bombardment, we treated the Pb_2GeS_4 crystal surface with Ar^+ ions (3000 V, 5 min duration, ion current density of $14.5 \mu\text{A}/\text{cm}^2$ and total Ar^+ flux was estimated to be about 5.4×10^{16} ions/ cm^2). Such experiments are of high interest because similar surface treatment is generally employed in different types of epitaxial techniques [19]. We used the same parameters of Ar^+ -ion surface treatment in a series of related Pb- and/or Ge-containing sulfides [16–18]. Further, measurements of the S $K\beta_{1,3}$ ($M_{\text{II,III}} \rightarrow K$ junction) and Ge $K\beta_2$ ($N_{\text{II,III}} \rightarrow K$ junction) XES bands yielding information on the energy

distribution of S 3p and Ge 4p electronic states, respectively, are made with apparatus energy resolution of about 0.3 eV using Johann-type DRS-2M spectrographs (BHV-7 X-ray tube, gold anode) following the technique reported elsewhere [20].

3 Calculating procedure

First-principles calculations of the electronic structure of Pb_2GeS_4 were performed by the augmented plane wave–local orbitals (APW–lo) method as incorporated in WIEN2k code [21]. In the present work we generally follow the technique reported in detail elsewhere [22]. The muffin-tin (MT) sphere radii for the atoms constituting Pb_2GeS_4 compound were used as following: 2.5 a.u. (Pb), 2.21 a.u. (Ge) and 1.90 a.u. (S) (note that 1 a.u. = 0.529177 \AA). It is worth mentioning that in spite of the fact that we use the term “MT sphere”, the peculiarity of the calculations employing the APW–lo method within the WIEN2k code is that the potential between the spheres is not constant [17]. Dimensions of the Pb_2GeS_4 unit-cell and the atomic positions are used in our calculations as they were established experimentally in Ref [4]. The $R_{\text{min}}^{\text{MT}}$ k_{max} parameter ($R_{\text{min}}^{\text{MT}}$ is the minimum MT sphere radius and k_{max} stands for the maximum k vector value in the plane wave expansion) is equal to 7.0, while the charge density is Fourier expanded up to $G_{\text{max}} = 12 \text{ (a.u.)}^{-1}$. In the case of potential decomposition, we extend the valence wave functions inside the MT spheres up to $l_{\text{max}} = 10$. In the present calculations, for exchange–correlation (XC) approximation, we use two commonly applied approaches, namely generalized gradient approximation (GGA) as developed by Perdew, Burke and Ernzerhof (PBE) [23] and modified Becke–Johnson (MBJ) potential [24]. We also use PBE and MBJ with Hubbard-corrected functional [25, 26] (PBE–U and MBJ–U approximations, respectively). In addition, since lead is considered a heavy element [27, 28], we involve also spin–orbit (SO) interaction in order to take into account relativistic effects. The SO interaction is taken into account employing the second variational method [29, 30] following the technique reported in detail elsewhere [17]. With the aim of integrating throughout the Brillouin zone (BZ) of Pb_2GeS_4 compound, we use the tetrahedron method as developed by Blöchl et al. [31]: in such a calculation procedure the BZ sampling is made involving 1000 k -points within the full zone. We verify the iteration procedure through changes in the integral charge difference $q = \int |\rho_n - \rho_{n-1}| dr$, where $\rho_{n-1}(r)$ and $\rho_n(r)$ are charge densities of previous iteration and current iteration, respectively, and the calculations were interrupted when reaching the value $q \leq 0.0001$. In Table 2 we summarize the group of atomic orbitals that were involved in the

Table 2 Atomic orbitals used in the present band-structure APW-*lo* calculations of Pb_2GeS_4

Atom	Core electrons	Semi-core electrons	Valence electrons	Quantity of semi-core and valence electrons involved in the present calculations
Pb	$1s^2 2s^2 2p^6 3s^2 3p^6 3d^{10}$ $4s^2 4p^6 4d^{10} 4f^{14} 5s^2$	$5p^6 5d^{10}$	$6s^2 6p^2$	20
Ge	$1s^2 2s^2 2p^6 3s^2 3p^6$	$3d^{10} 4s^2$	$4p^2$	14
S	$1s^2 2s^2 2p^6$	$3s^2$	$3p^4$	6

present DFT calculations of Pb_2GeS_4 compound. However, the core electrons are not “frozen” in the APW-*lo* method and they are taken into account in the present calculations as well.

With respect to the key optical constants calculated in the present work for Pb_2GeS_4 , the complex dielectric function $\epsilon(\omega) = \epsilon_1(\omega) + i\epsilon_2(\omega)$, which thereby relates to the band structure of solids, should involve both inter-band and intra-band transitions; however, we omit the latter transitions because they are significant only in the case of metals [32]. Therefore, we consider only the direct transitions between the valence band (VB) and the conduction band (CB) and phonon contribution into the indirect-band transitions is not taken into account. The Kramers–Kronig dispersion equation is used to derive the real part of dielectric function $\epsilon_1(\omega)$ from the $\epsilon_2(\omega)$ function [33], while the principal optical constants (absorption coefficient, refractive index, extinction coefficient, optical reflectivity coefficient, and electron energy-loss spectrum) are elucidated in the present work for the Pb_2GeS_4 compound using well-known equations which include the $\epsilon_1(\omega)$ and $\epsilon_2(\omega)$ functions exactly as they were reported in Ref [34].

4 Results and discussion

4.1 XPS measurements

We present in Fig. 5 the survey XPS spectra measured for the as-synthesized and treated with Ar^+ -ions surfaces of the Pb_2GeS_4 crystal. All specific features of the survey XPS spectra are well ascribed to the presence of lead, germanium and sulfur atoms, which constitute the ternary sulfide under study. The exceptions are only the 1s levels and the KLL Auger lines related to carbon and oxygen that are due to hydrocarbons and oxygen-containing species adsorbed from laboratory air (before we started the XPS measurements, the as-grown Pb_2GeS_4 crystal surface was exposed to air over several weeks). However, comparative intensities of the C 1s and O 1s lines are rather low for the as-grown Pb_2GeS_4 crystal surface, and their relative intensities on the XPS spectrum decrease abruptly after treatment with Ar^+ -ions. As Fig. 5 presents, in the latter case, rather low-intensive

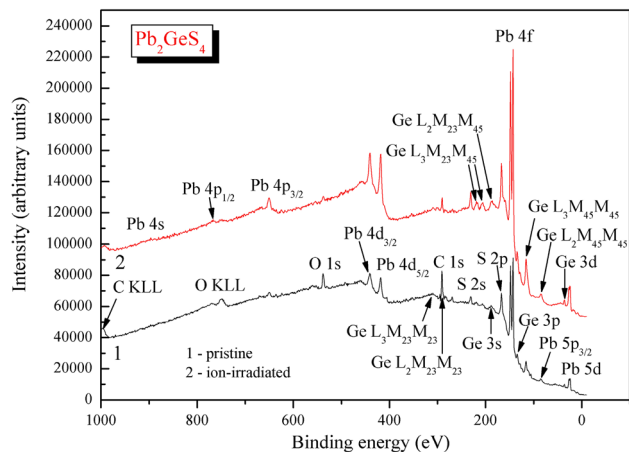


Fig. 5 Survey XPS spectra of (1) as-synthesized and (2) treated with Ar^+ -ions surfaces of the Pb_2GeS_4 crystal

C 1s and O 1s core-level spectra are detected in the uppermost surface layers of the Pb_2GeS_4 crystal. The above data reveal comparatively low hygroscopicity of the Pb_2GeS_4 crystal surface. Low hygroscopicity was established to be a characteristic feature also of other Pb- and/or Ge-containing sulfides, in particular $\text{Ag}_{0.5}\text{Pb}_{1.75}\text{GeS}_4$ [15], $\text{Ag}_2\text{In}_2\text{GeS}_6$ [16], $\text{Ag}_2\text{PbGeS}_4$ [17], $\text{TlInGe}_3\text{S}_8$ [18].

The most informative core-level XPS spectra of lead, germanium and sulfur are presented in Fig. 6, while Fig. 7 presents the XPS VB spectrum of this crystal. The XPS spectra in the above figures are plotted for both as-grown and treated with Ar^+ -ions Pb_2GeS_4 crystal surfaces. Comparison of the BE values of the Pb 4f(4d) and Ge 3d core-level electrons of Pb_2GeS_4 (Table 3) with literature data [35–37] indicates that the charge state of lead in the crystal under consideration is close to +2, while that of germanium is smaller than +4. The present XPS measurements indicate that the treatment of the Pb_2GeS_4 crystal surface with Ar^+ -ions possessing the total Ar^+ flux of about 5.4×10^{16} ions/cm² did not cause changes in stoichiometry and the BE values of the core-level electrons (Table 3) as well as in the shapes of the XPS core-level and VB spectra (see Figs. 6, 7). Therefore, the Pb_2GeS_4 crystal surface is quite stable with respect to the treatment with Ar^+ -ions. Analogous conclusion was made previously when applying the same Ar^+ -ion treatment

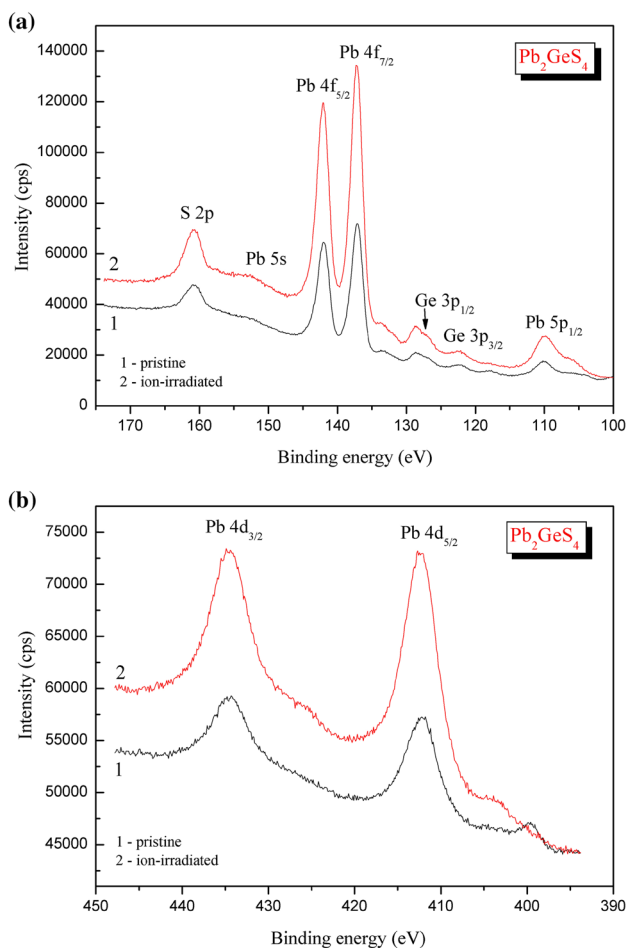


Fig. 6 XPS core-level spectra of (1) as-synthesized and (2) treated with Ar⁺-ions surfaces of the Pb₂GeS₄ crystal: **a** S 2p, Pb 4f, Ge 3p, Pb 5p and **b** Pb 4d

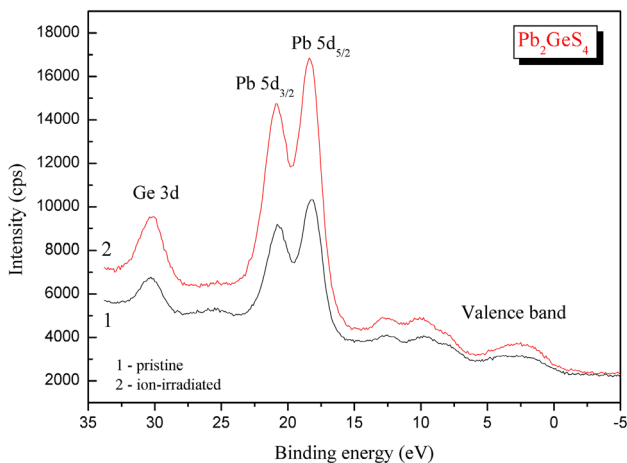


Fig. 7 XPS VB spectra of (1) as-synthesized and (2) treated with Ar⁺-ions surfaces of the Pb₂GeS₄ crystal

Table 3 Binding energies (in eV^{*}) of constituent element core levels of as-synthesized and treated with Ar⁺-ions surfaces of the Pb₂GeS₄ crystal

Core-level	Pb ₂ GeS ₄ /as-synthesized surface	Pb ₂ GeS ₄ /treated with Ar ⁺ -ions surface
Pb5d _{5/2}	18.27	18.34
Pb5d _{3/2}	20.73	20.79
Ge 3d	30.29	30.24
Pb 4f _{7/2}	137.13	137.22
Pb 4f _{5/2}	142.43	142.46
S 2p	160.71	160.78
Pb 4d _{5/2} **	412.4	412.5
Pb 4d _{3/2} **	434.5	434.6

*Uncertainty of the measurements is ±0.05 eV

**Uncertainty of the measurements is ±0.1 eV

technique in the case of the related sulfide, Ag_{0.5}Pb_{1.75}GeS₄, in which part of lead atoms are substituted by silver atoms (with some additional content of the former atoms as well) [15]. However, further increase of the silver content in the Ag₂PbGeS₄ compound was found to cause the unstablens of its surface. Ar⁺-ion treatment of the Ag₂PbGeS₄ crystal surface causes decreasing the silver content in its topmost crystal surface layers by about 34% [17]. The analogous effect of decreasing the silver content was observed previously for several Ag, Ge, and S-containing semiconductors, in particular Ag₂In₂GeS₆ [16] and AgGaGeS₄ [38].

4.2 Electronic structure based on DFT calculations and X-ray spectroscopy measurements

Figure 8 presents total DOS of Pb₂GeS₄ as obtained in the present DFT calculations using GGA, GGA–U, MBJ, and MBJ–U–SO approaches. It is apparent that the main peculiarities of total DOS curves within the energy region corresponding to sub-bands marked as A to E in Fig. 8 are similar to each other with respect to their shapes and energy positions irrespective of the XC approximation used in the present calculations. However, the energy positions of the band corresponding to Pb 5d states in the calculations using the GGA [23] and MBJ [24] techniques are shifted toward the Fermi level by about 2.0 and 1.5 eV, respectively, as compared with the position of the feature F of the experimental XPS VB spectrum of the Pb₂GeS₄ crystal. Furthermore, the calculations made within the GGA technique reveal somewhat underestimated energy band gap (E_g = 1.880 eV), while that obtained within the MBJ technique is somewhat overestimated (E_g = 2.558 eV; see Table 4) in comparison with E_g = 2.29 ± 0.01 eV as established experimentally in Ref [6], for Pb₂GeS₄ compound. We believe that the mentioned difference of the shape and energy positions of basic

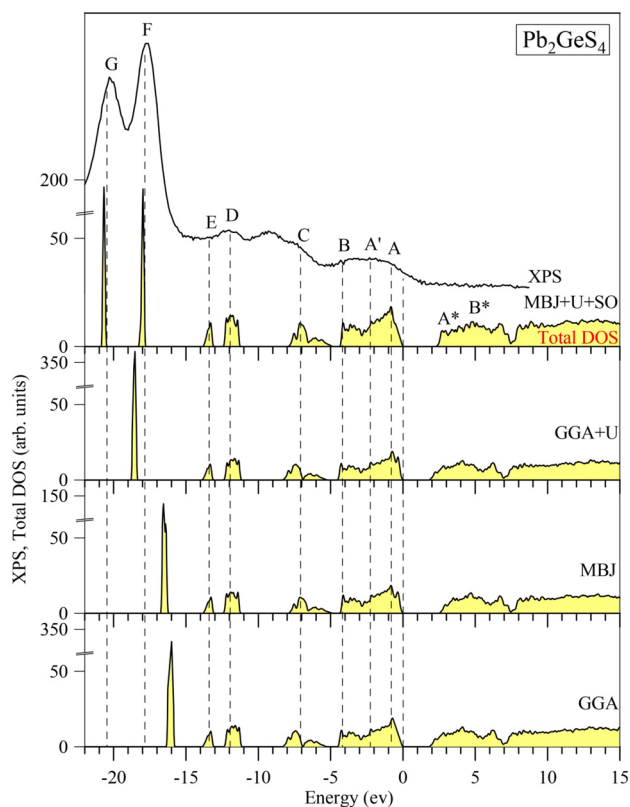


Fig. 8 Curves of total DOS calculated for Pb_2GeS_4 within the GGA, GGA+U, MBJ, and MBJ+U+SO approximations matched on a joint energy scale with the XPS VB spectrum of the studied compound

Table 4 Band gap energies of Pb_2GeS_4 as derived in the DFT calculations in comparison with experimental measurements

Method of calculation	E_g (theory)	E_g (experiment)
GGA	1.880 eV	2.29 ± 0.01 eV [6]
GGA+U	1.882 eV	
MBJ	2.558 eV	
MBJ+U+SO	2.364 eV	

peculiarities of the curve of total DOS and the experimental XPS VB spectrum of the Pb_2GeS_4 crystal can be interpreted by neglecting highly correlated d electrons in the GGA technique [23]. This problem can be generally solved by adopting the GGA+U technique [25, 26] by involving the correction parameter U. The addition of this parameter for highly correlated electrons generally allows adjusting theoretical DOS curves to experimental XPS spectra [22, 39]. In the present work we employ $U = 0.43$ Ry for Pb 5d electrons when calculating the electronic band-structure of Pb_2GeS_4 within the GGA+U technique [25, 26]. Figure 8 presents that the addition of this parameter in our calculations does not affect significantly the total DOS curve within the VB and

CB regions; although this XC approximation allows moving the position of the Pb 5d band away from E_F . Nevertheless, the E_g value in this case is again far underestimated as compared to that obtained experimentally (1.882 eV vs. 2.29 eV; Table 4). Application in our calculations of MBJ potential [24] gives an underestimated position of the Pb 5d band in the theoretical DOS curve (Fig. 8) and overestimated energy band gap (2.558 eV; see Table 4) as reported above. Since lead atom is recognized to be a heavy element [27, 28], the SO interaction effect is worth considering [40–42]. Our calculations within MBJ potential [24] involving both the correction parameter $U = 0.43$ Ry for Pb 5d electrons as well as the SO interaction effect (MBJ+U+SO) are presented in Fig. 8. It is apparent that data of the band-structure calculations made within the MBJ+U+SO approximation reveal good agreement of the total DOS curve with the experimental XPS VB spectrum regarding the shape and energy positions of the main peculiarities (the hump at about 9.5 eV detected in the experimental XPS VB spectrum which does not appear in the theoretical DOS curve is interpreted by the excitation of the Pb $5d_{5/2}$ core-level spectrum by Mg $K\alpha_3$ satellite [43, 44]). The calculations performed within the MBJ+U+SO approximation yield the value of 2.5 eV for SO splitting of the XPS Pb $5d_{5/2,3/2}$ core-level electrons in Pb_2GeS_4 , which is in excellent agreement with the experimental findings (Table 3). Furthermore, the band gap energy value obtained in our MBJ+U+SO calculations ($E_g = 2.364$ eV; Table 4) is in good agreement with the experimental E_g value [6].

Detailed PDOS curves of Pb, Ge and S atoms in Pb_2GeS_4 within the MBJ+U+SO approximation are plotted in Fig. 9. The calculations yield that the Pb_2GeS_4 VB region extends from 0 to about 8.0 eV and the band consists of several sub-bands, marked as A, A', B, and C in Fig. 9. The main contribution to the upper sub-band A is derived from S 3p states, with smaller contribution of Pb 6s states as well. The main contributors to the sub-band A' of the Pb_2GeS_4 VB are again S 3p states, with somewhat smaller contributions of Pb 6p and Ge 4p states too, while the sub-band B is formed mainly by S 3p and Ge 4p states in almost equal proportion. The bottom of the VB of Pb_2GeS_4 (sub-band C) is dominated by Pb 6s states, with somewhat smaller contributions of Ge 4s states. Some minor contributions of S 3p states in the sub-band C are also detected by the present DFT calculations of Pb_2GeS_4 (see Fig. 9). Further, the band D centered at about 11.9 eV is dominated by S 3s states, with smaller contributions of Ge 4p states, while Ge 4s and S 3s states are main contributors to the lower band E centered at about 13.3 eV. In addition, the lowest bands F and G resolved in the XPS spectrum plotted in Fig. 8 are Pb $5d_{5/2}$ and Pb $5d_{3/2}$ states, respectively. The bottom of the CB (sub-band A*, Fig. 9) is composed mainly by unoccupied Pb 6p states, with smaller contributions of Ge 4s* and S 3p* states too.

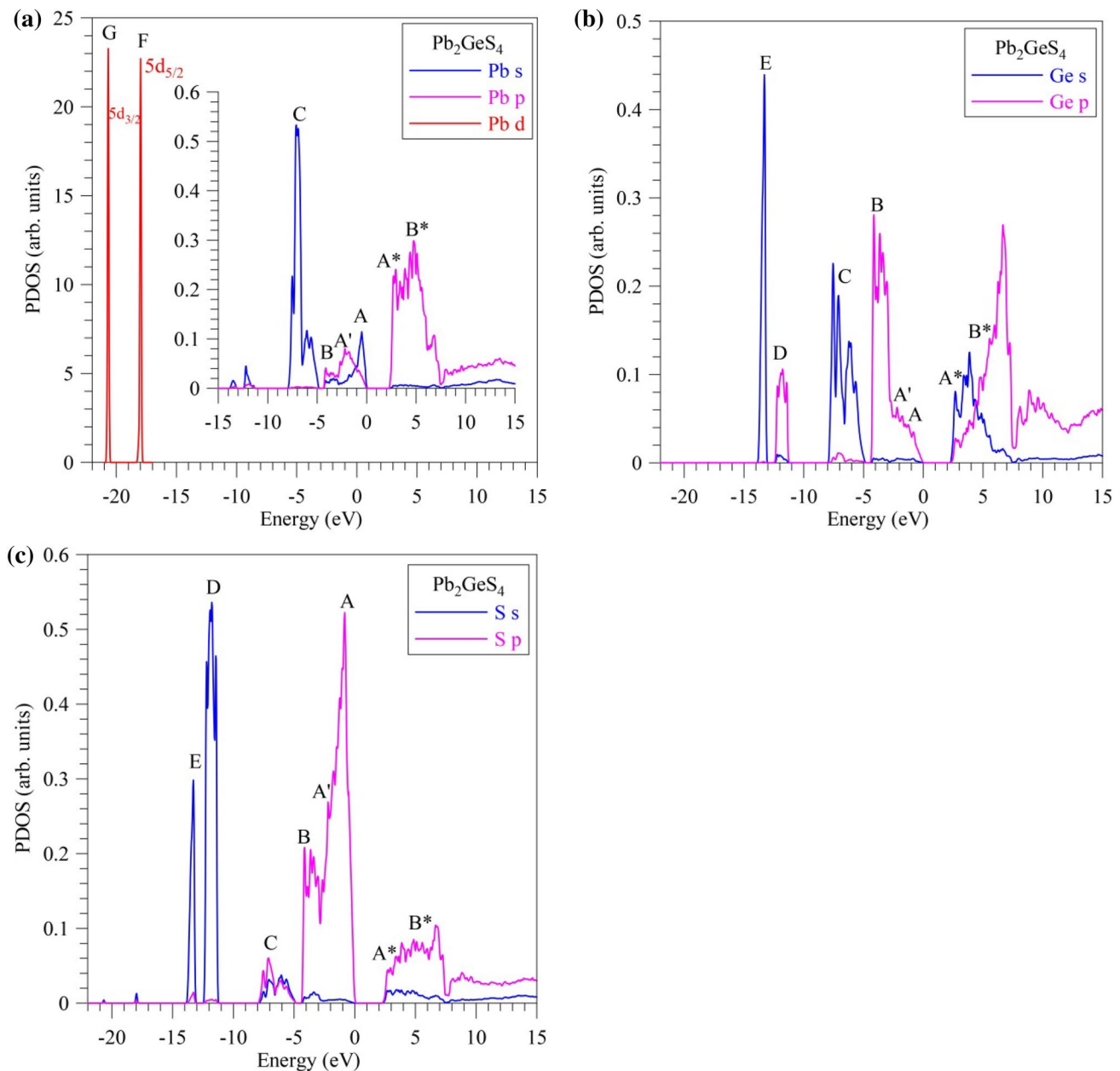


Fig. 9 Partial densities of states of **a** Pb, **b** Ge and **c** S atoms of Pb_2GeS_4 (calculated with MBJ–U–SO approximation)

The present band-structure calculations reveal that S 3p states are significantly hybridized with Ge 4p states in the energy region corresponding to the sub-band B, and substantial hybridization of Ge 4s states with Pb 6s and Ge 4p states at the bottom of the Pb_2GeS_4 VB (sub-band C) is also observed (Fig. 9). The existence of hybridization of the mentioned electronic states suggests a significant contribution of the covalent component of the chemical bonding of Pb_2GeS_4 compound (additionally to the ionic component). Altogether, S 3p states are the main contributors to the VB of Pb_2GeS_4 locating in its upper and central

portions, while the principal contributors to its bottom are Pb 6s states.

The above data on the occupation of the VB region by S 3p and Ge 4p states are confirmed experimentally for the Pb_2GeS_4 crystal by measurements of the S $\text{K}\beta_{1,3}$ and Ge $\text{K}\beta_2$ X-ray emission bands yielding information on the valence S 3p and Ge 4p state energy distribution. The above XES bands are compared in Fig. 10 on a common energy scale with its XPS VB spectrum following the technique reported elsewhere [45, 46] that is generally used when comparing XPS and XES spectra in order to probe features of filling the

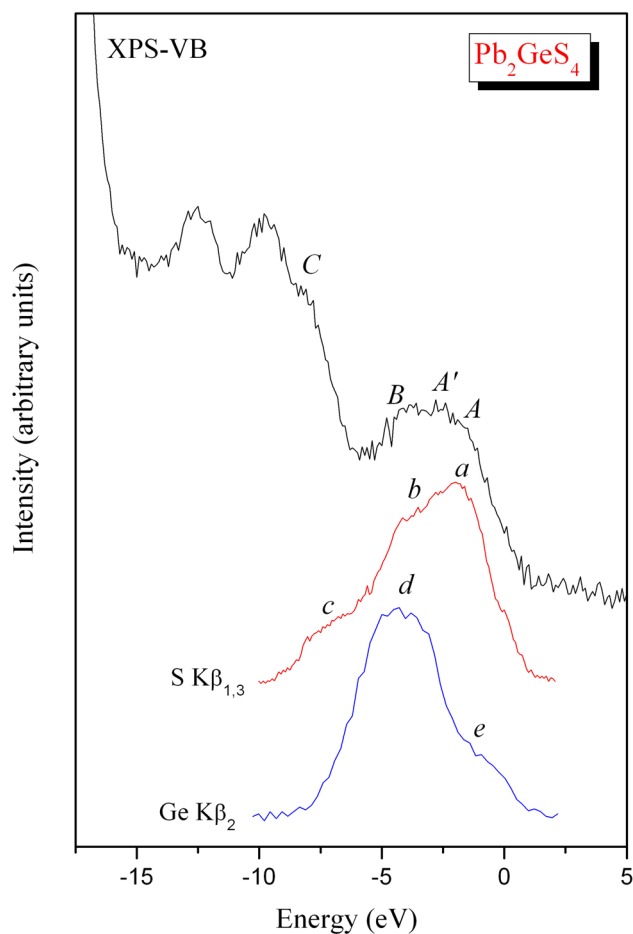


Fig. 10 Comparison on a joint energy scale of the XPS VB spectrum and the Ge $\text{K}\beta_2$ and S $\text{K}\beta_{1,3}$ X-ray emission bands of the Pb_2GeS_4 crystal

VB region by electronic states associated with constituting atoms [47, 48]. In such a comparison, the zero of energy of the X-ray spectroscopy spectra plotted in Fig. 10 for the Pb_2GeS_4 crystal fits to the Fermi energy position of the PHOIBOS 150 energy analyzer used in the UHV-Analysis-System. The energy position of the main maximum a of the S $\text{K}\beta_{1,3}$ X-ray emission band corresponds to the top of the XPS VB spectrum, while the positions of the peculiarities b and c of this XES band correspond to the features B and C of the XPS spectrum. Further, the main maximum d of the Ge $\text{K}\beta_2$ X-ray emission band coincides with the peculiarity B of the XPS VB spectrum (Fig. 10). The above experimental X-ray spectroscopy findings are in good agreement with the results of band-structure calculations of the compound under consideration presented in Fig. 9. Certainly, significant contributions of Pb 6s and Ge 4s states in the vicinities of the features C and B of the XPS VB spectrum are expected to occur in accordance with the present theoretical predictions shown in Fig. 9; however, available experimental abilities do not allow us to perform measurements of the energy

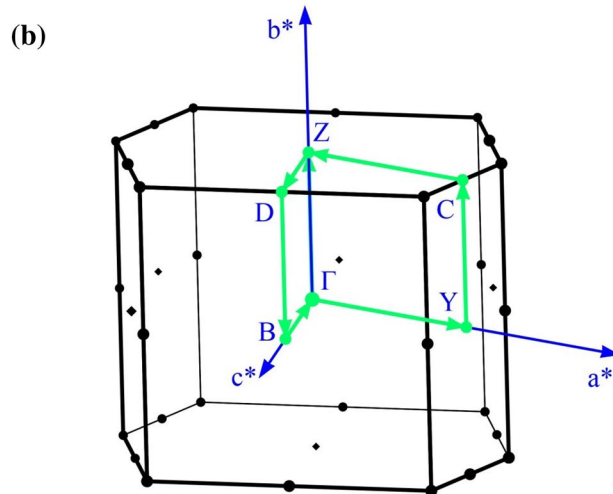
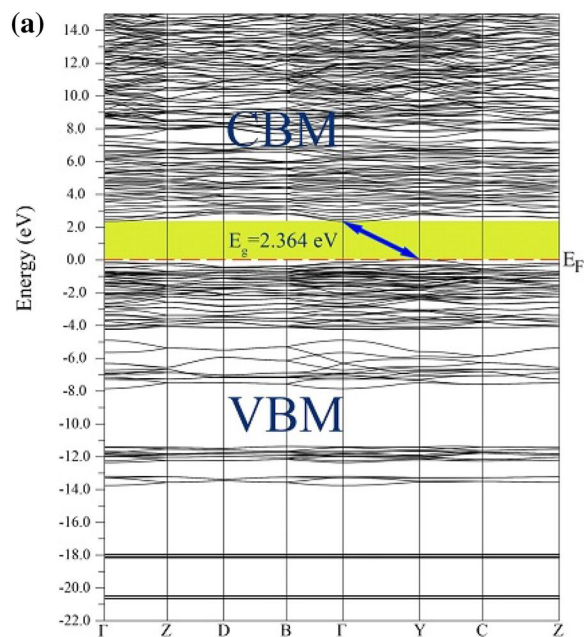


Fig. 11 a Electronic bands at broad special symmetry paths within the first BZ and **b** diagram of the BZ for a monoclinic structure, in which Pb_2GeS_4 compound is crystallized

distribution of the above electronic states in the Pb_2GeS_4 crystal.

Band dispersions for special symmetry points and directions of Pb_2GeS_4 are shown in Fig. 11a, while coordinates of the k points within the restricted monoclinic BZ (Fig. 11b) are as follows: Γ (0.0, 0.0, 0.0), Z (0.0, 0.5, 0.0), D (0.0, 0.5, 0.5), B (0.0, 0.0, 0.5), Γ (0.0, 0.0, 0.0), Y (0.5, 0.0, 0.0), C (0.5, 0.5, 0.0) and Z (0.0, 0.5, 0.0). Figure 11a presents that the band dispersions are comparably flat in the k space near the VB maximum (VBM) and CB minimum (CBM). This fact suggests high effective masses and low electron mobility in Pb_2GeS_4 compound. Our calculations yield that the VBM

is positioned at the Y point, while the CBM at the Γ point indicating that the ternary sulfide Pb_2GeS_4 is an indirect-gap semiconductor. It is worth mentioning that the DFT calculations of the other ternary sulfide occurring in the PbS-GeS_2 system, namely PbGeS_3 , also reveal its indirect gap [2].

4.3 DFT calculations of the basic optical parameters

Results of the present calculations of the absorption coefficient $\alpha(\omega)$ within the MBJ–U–SO approximation (Fig. 12) show that the edge of optical absorption (first critical point) appears in Pb_2GeS_4 at about 2.36 eV and, with a further increase of photon energy, it increases rapidly above the edge. The range of strong absorption [magnitudes of $\alpha(\omega)$ are bigger than 10^4 cm^{-1}] in Pb_2GeS_4 is detected for broad photon energy area, from about 4 eV up to 27 eV. The existence of high values of the absorption coefficient $\alpha(\omega)$ in the broad energy region suggests that Pb_2GeS_4 compound is a promising semiconductor for the use in thin-film solar cells, while the existence of well-distinguished spectral peaks/humps on the $\alpha(\omega)$ curve originating due to different electronic transitions reveals its prospects for optoelectronic applications.

The real part of dielectric function $\epsilon_1(\omega)$ of Pb_2GeS_4 is presented in Fig. 13a, while the imaginary part of dielectric function $\epsilon_2(\omega)$ is shown in Fig. 13b. The $\epsilon_1(\omega)$ curve reveals the existence of three features, A (~ 3 eV), B (~ 5 eV), and C (~ 8.5), while the energy positions of the similar fine-structure peculiarities resolved on the $\epsilon_2(\omega)$ curve are slightly different (A (~ 4 eV), B (~ 6 eV), and C (~ 9 eV)). Values

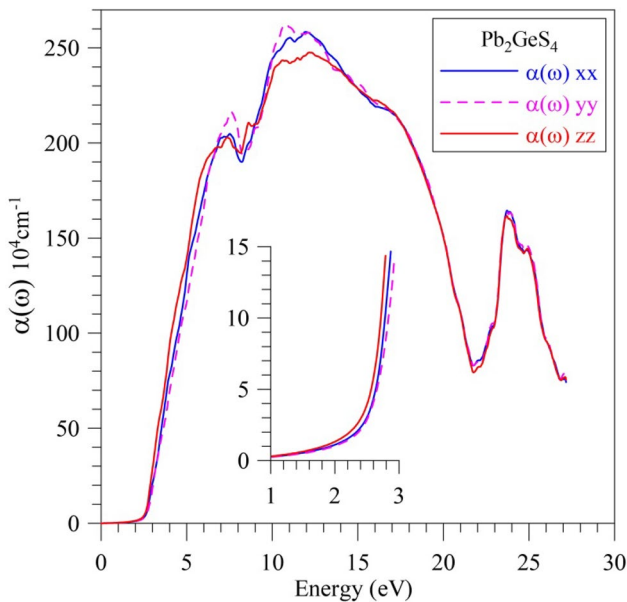


Fig. 12 Calculated absorption coefficient $\alpha(\omega)$ of Pb_2GeS_4 (MBJ–U–SO approximation)

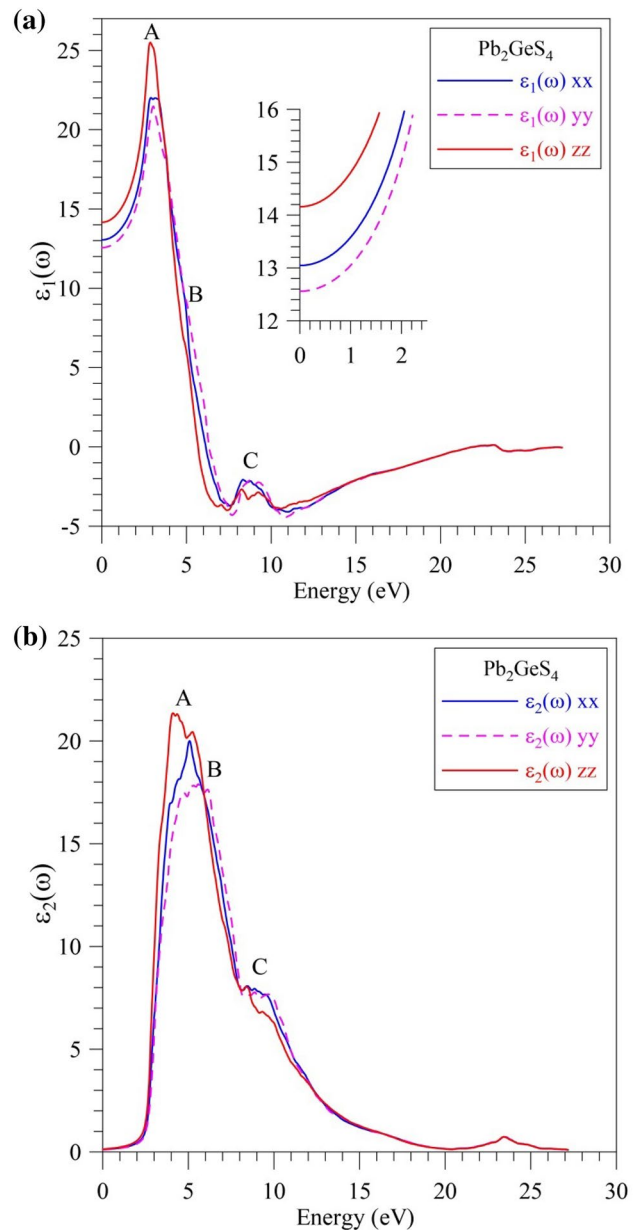


Fig. 13 Calculated **a** real and **b** imaginary parts of dielectric function ($\epsilon_1(\omega)$ and $\epsilon_2(\omega)$, respectively) of Pb_2GeS_4 (MBJ–U–SO approximation)

of static dielectric constants of Pb_2GeS_4 at zero frequency in accordance with the present calculations are as follows: $\epsilon_1^{xx}(0) = 13.0474$, $\epsilon_1^{yy}(0) = 12.5604$ and $\epsilon_1^{zz}(0) = 14.1584$. Figure 13a presents that the calculated real part of dielectric function $\epsilon_1(\omega)$ of Pb_2GeS_4 reveals a sharp decrease beginning from about 3 eV till 7.5 eV and, then, revealing a well-resolved feature C at 8.5 eV, it increases with an increase of photon energy till ~ 27 eV. The calculated imaginary part of dielectric function $\epsilon_2(\omega)$ decreases beginning from ~ 4 eV and yields a tendency toward approaching zero at about 27 eV with the presence of a small shoulder B and

a fine-structure peculiarity C (Fig. 13b). Following data of the theoretical calculations of PDOSs curves presented in Fig. 9, it is suggested that the peculiarities A–C observed on the curve of the imaginary part of dielectric function $\epsilon_2(\omega)$ originate due to the following electronic transitions: Pb(s)→Pb(p), Pb(p)→Pb(s), Ge(s)→Ge(p), Ge(p)→Ge(s), S(s)→S(p) and S(p)→S(s). This designation considers only inter-band transitions which obey the dipole selection rules regarding the matrix elements of the transition probabilities as reported elsewhere [17]. Figure 14a presents calculated

refractive index $n(\omega)$ of Pb_2GeS_4 . Comparing this figure with the real part of dielectric function $\epsilon_1(\omega)$ presented in Fig. 13a, one can see some similarity of the $n(\omega)$ and $\epsilon_1(\omega)$ curves with respect to the contours and energy positions of the peculiarities A–C for photon energies ranging from 0 to about 11 eV. The values of the $n(\omega)$ index of Pb_2GeS_4 compound at zero frequency are as follows: $n^{xx}(0) = 3.612$, $n^{yy}(0) = 3.544$, and $n^{zz}(0) = 3.763$. Maximum values of the refractive index $n(\omega)$ in the compound under discussion are detected in the energy range of 0–5.5 eV. The $n(\omega)$ function

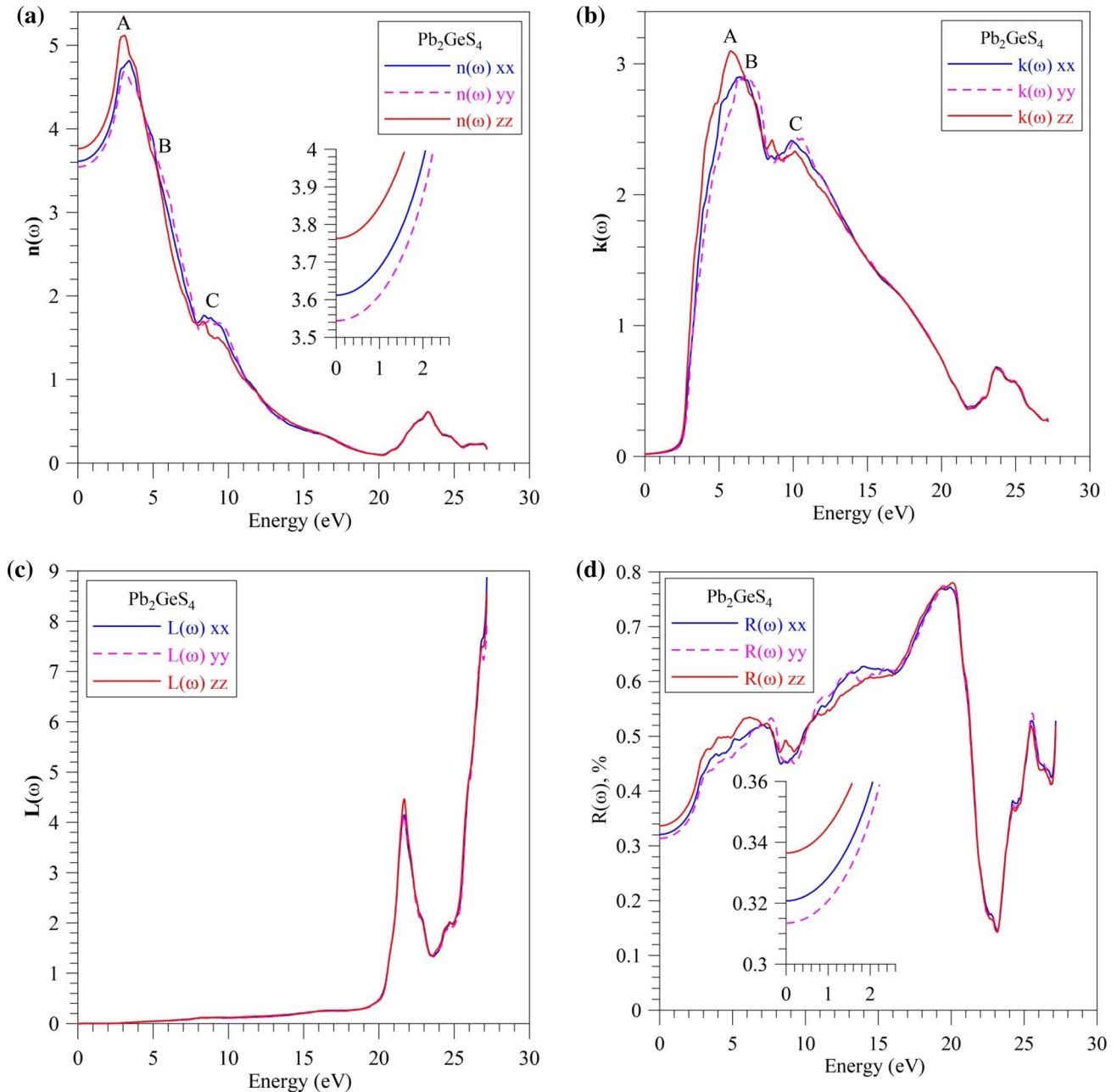


Fig. 14 Calculated **a** refractive index $n(\omega)$, **b** extinction coefficient $k(\omega)$, **c** electron energy-loss spectrum $L(\omega)$, and **d** optical reflectivity $R(\omega)$ of Pb_2GeS_4 (MBJ–U–SO approximation)

decreases beginning from about 3.5 eV till 20.5 eV and shows a well-resolved sub-band centered at about 23 eV. Data of the calculations of the extinction coefficient $k(\omega)$ of Pb_2GeS_4 are shown in Fig. 14b. The $k(\omega)$ function in Pb_2GeS_4 reveals some similarity of trends for changes in its shape and fine-structure formation as it was detected in the case of the curve of the imaginary part of dielectric function $\epsilon_2(\omega)$ (cf. Figs. 13b, 14b).

Energy-loss spectrum $L(\omega)$ of Pb_2GeS_4 that gives information on the energy loss of fast-moving electrons is plotted in Fig. 14c. The $L(\omega)$ function increases very smoothly in Pb_2GeS_4 till 20 eV and yields a sharp increase resulting in the appearance of a peak around 21.5 eV followed by fast decrease till about 23.5 eV. At higher photon energies the energy-loss spectrum $L(\omega)$ increases again. The maximum at 21.5 eV observed on the $L(\omega)$ curve can be ascribed to the plasma frequency in the Pb_2GeS_4 compound. For calculated photon energies, the energy-loss spectrum $L(\omega)$ yields very minor anisotropy of different tensor components (xx, yy, zz) in Pb_2GeS_4 (Fig. 14c). Data of our calculations of optical reflectivity coefficient $R(\omega)$ (Fig. 14d) reveal three non-zero components corresponding to the reflections at 0 eV as follows: $R^{xx}(0)=32.078\%$, $R^{yy}(0)=31.346\%$, and $R^{zz}(0)=33.650\%$, while maximum reflectivity 78.016% is detected at around 20.07 eV. Finally, it should be indicated that the principal optical constants calculated in the present work exhibit comparatively large isotropic behavior of the three components of the tensor (xx, yy, zz).

The above data indicate that Pb_2GeS_4 belongs to such kind of materials that are very promising for the laser induced effects and optical memory devices. Furthermore, the presence of possible intrinsic defects in the Pb_2GeS_4 crystal should influence somewhat the optical constants calculated in the present work. Since we have studied these constants only based on DFT calculations, we leave this task for future experimental studies. In addition, big electron–phonon anharmonicity is very crucial in this material.

5 Conclusions

The electronic band-structure of Pb_2GeS_4 compound was studied in the present work using both experimental and theoretical methods. Notably, for the Pb_2GeS_4 single crystal grown by Bridgman–Stockbarger method we have recorded the XPS core-level spectra for the atoms constituting the crystal in order to determine their electron binding energies. The XPS measurements were made for the as-synthesized and treated with Ar^+ -ions surfaces of the Pb_2GeS_4 crystal. These measurements yield that this surface treatment does not cause changes in the BE values of the core-level electrons of atoms constituting the Pb_2GeS_4 crystal. This surface treatment does not change the shape of the XPS VB

spectrum as well as stoichiometry of the crystal surface. The Pb_2GeS_4 crystal surface is rather stable with respect to the treatment with Ar^+ -ions and it reveals low hygroscopicity. Such properties can be of significant importance when using this crystal in optoelectronic devices operating at ambient conditions. DFT calculations made within the APW–lo method as incorporated in WIEN2k code demonstrate that the best fit with the experimental XPS VB spectrum of the Pb_2GeS_4 crystal is derived using XC approximation of MBJ potential with Hubbard-corrected functional and taking into account SO interaction. Our calculations indicate that the top and upper portion of the VB of Pb_2GeS_4 is dominated by S 3p states, Ge 4p and S 3p states are the main contributors to the central portion of the band, while its bottom is dominated by Pb 6s states with slightly smaller contributions of Ge 4s states. Further, the bottom of the CB of Pb_2GeS_4 is dominated by unoccupied Pb 6p states, with somewhat smaller contributions of Ge 4s* and S 3p* states. The above theoretical prediction of the filling of the VB by Ge 4p and S 3p states has been confirmed experimentally by the matching on a common energy scale of the XPS VB spectrum and the S $\text{K}\beta_{1,3}$ and Ge $\text{K}\beta_2$ X-ray emission bands giving information on the valence S p and Ge p states, respectively. Our calculations demonstrate a significant contribution of the covalent component of the chemical bonding in Pb_2GeS_4 compound (additionally to the ionic component). The DFT calculations indicate that the Pb_2GeS_4 semiconductor is of indirect-gap nature because its VBM and CBM are positioned at the Y and Γ points, respectively.

The basic optical constants are also elucidated using the ab initio DFT calculations. The present calculations show that the edge of optical absorption (first critical point) arises at about 2.36 eV and, with the further increase of photon energy, it increases rapidly above the edge. The presence of high values of the absorption coefficient $\alpha(\omega)$ in the broad energy region indicates that Pb_2GeS_4 compound is a promising semiconductor for the use in thin-film solar cells, while the presence of well-distinguished spectral peaks/humps on the $\alpha(\omega)$ curve originating due to different electronic transitions is rather prospective for optoelectronic application. The static dielectric constants as calculated in the present work for the $\epsilon_1(\omega)$ function are as follows: $\epsilon_1^{xx}(0)=13.0474$, $\epsilon_1^{yy}(0)=12.5604$ and $\epsilon_1^{zz}(0)=14.1584$. Some similarity of the $n(\omega)$ and $\epsilon_1(\omega)$ curves with respect to the shapes and energy positions of the fine-structure peculiarities for photon energies ranging from 0 to about 11 eV is detected for Pb_2GeS_4 compound, while the $k(\omega)$ function reveals some similarity of changing its shape and fine-structure formation with the imaginary part of dielectric function $\epsilon_2(\omega)$. The maximum at 21.5 eV observed on the $L(\omega)$ curve can be ascribed to plasma frequency in Pb_2GeS_4 . Calculated optical reflectivity coefficient $R(\omega)$ reveals its maximum at around 20.07 eV. The present results allow the conclusion that Pb_2GeS_4

belongs to such kind of materials that are very promising for the laser induced effects and optical memory devices. Certainly, the presence of intrinsic defects can somewhat influence the calculated optical constants and the existence of big electron–phonon anharmonicity is very crucial in this compound.

References

- D.I. Bletskan, *Crystalline and Glassy Chalcogenides of Si, Ge, Sn and Alloys on their Base (Volume 1)* (Zakarpattia, Uzhhorod, 2004)
- M.M. Bletskan, D.I. Bletskan, V.M. Kabatsii, *Quantum Electron. Optoelectron.* **18**, 12–19 (2015)
- M. Elli, A. Mugnoli, *Atti Accad. Naz. Lincei, Rend. Cl. Sci. Fis. Mat. Nat.* **33**, 316 (1962)
- K. Susa, H. Steinfink, *J. Solid State Chem.* **3**, 75–82 (1971)
- M. Ribes, J. Olivier-Fourcade, E. Philippot, M. Maurin, *Acta Cryst. B* **30**, 1391–1395 (1974)
- D.I. Bletskan, V.P. Terban, M.I. Gurzan, M.V. Potorii, *Inorg. Mater.* **26**, 509–514 (1990)
- Z.V. Popović, *Phys. B* **119**, 283–289 (1983)
- D.I. Bletskan, Yu.V. Voroshilov, L.M. Durdinets, P.P. Migalko, V.A. Stefanovich, V.N. Kabatsii, *Cryst. Rep.* **48**, 624–626 (2003)
- K.M. Poduska, L. Cario, F.J. DiSalvo, K. Min, P.S. Halasyamani, *J. Alloys Compd.* **335**, 105–110 (2002)
- G.H. Moh, *Neues Jahrbuch für Mineralogie. Abhandlungen* **128**, 115–188 (1977)
- R.G. Taylor, *Geology of Tin Deposit, Vol. 11* (Elsevier, Amsterdam, 1979)
- V.V. Atuchin, O.Y. Khyzhun, O.D. Chimitova, M.S. Molokeev, T.A. Gavrilova, B.G. Bazarov, J.G. Bazarova, *J. Phys. Chem. Solids* **77**, 101–108 (2015)
- O.Y. Khyzhun, V.L. Bekenev, V.V. Atuchin, L.D. Pokrovsky, V.N. Shlegel, N.V. Ivannikova, *Mater. Des.* **105**, 315–322 (2016)
- S.F. Solodovnikov, V.V. Atuchin, Z.A. Solodovnikova, O.Y. Khyzhun, M.I. Danylenko, D.P. Pishchur, P.E. Plyusnin, A.M. Pugachev, T.A. Gavrilova, A.P. Yelissev, A.H. Reshak, Z.A. Alahmed, N.F. Habubi, *Inorg. Chem.* **56**, 3276–3286 (2017)
- Y. Kogut, O.Y. Khyzhun, O.V. Parasyuk, A.H. Reshak, G. Lakshminarayana, I.V. Kityk, M. Piasecki, *J. Cryst. Growth* **354**, 142–146 (2012)
- A.H. Reshak, O.Y. Khyzhun, I.V. Kityk, A.O. Fedorchuk, H. Kamarudin, S. Auluck, O.V. Parasyuk, *Sci. Adv. Mater.* **5**, 316–327 (2013)
- T.V. Vu, A.A. Lavrentyev, B.V. Gabrelian, V.A. Ocheretova, O.V. Parasyuk, O.Y. Khyzhun, *Mater. Chem. Phys.* **208**, 268–280 (2018)
- O.Y. Khyzhun, A.O. Fedorchuk, I.V. Kityk, M. Piasecki, M.Y. Mozolyuk, L.V. Piskach, O.V. Parasyuk, A.M. ElNaggar, A.A. Albassam, P. Karasinski, *Mater. Chem. Phys.* **204**, 336–344 (2018)
- V.V. Atuchin, E.N. Galashov, O.Y. Khyzhun, V.L. Bekenev, L.D. Pokrovsky, Y.A. Borovlev, V.N. Zhdankov, *J. Solid State Chem.* **236**, 24–31 (2016)
- O.Y. Khyzhun, Y.V. Zaulychny, E.A. Zhurakovsky, *J. Alloys Compd.* **244**, 107–112 (1996)
- P. Blaha, K. Schwarz, G.K.H. Madsen, D. Kvasnicka, J. Luitz, *WIEN2k, An Augmented Plane Wave + Local Orbitals Program for Calculating Crystal Properties* (Karlheinz Schwarz, Technical Universität Wien, Wien, 2001) (ISBN 3-9501031-1-2)
- T.V. Vu, A.A. Lavrentyev, B.V. Gabrelian, O.V. Parasyuk, V.A. Ocheretova, O.Y. Khyzhun, *J. Alloys Compd.* **732**, 372–384 (2018)
- J.P. Perdew, S. Burke, M. Ernzerhof, *Phys. Rev. Lett.* **77**, 3865–3868 (1996)
- F. Tran, P. Blaha, *Phys. Rev. Lett.* **102**, 226401 (2009)
- V.I. Anisimov, I.V. Solov'yev, M.A. Korotin, M.T. Czyżyk, G.A. Sawatzky, *Phys. Rev. B* **48**, 16929–16934 (1993)
- P. Novák, F. Boucher, P. Gressier, P. Blaha, K. Schwarz, *Phys. Rev. B* **63**, 235114 (2001)
- V.L. Bekenev, O.Y. Khyzhun, A.K. Sinelnichenko, V.V. Atuchin, O.V. Parasyuk, O.M. Yurchenko, Y. Bezsmolnyy, A.V. Kityk, J. Szkutnik, S. Calus, *J. Phys. Chem. Solids* **72**, 705–713 (2011)
- O.Y. Khyzhun, V.L. Bekenev, O.V. Parasyuk, S.P. Danylchuk, N.M. Denysyuk, A.O. Fedorchuk, N. AlZayed, I.V. Kityk, *Opt. Mater.* **35**, 1081–1089 (2013)
- D.D. Koelling, B.N. Harmon, A technique for relativistic spin-polarised calculations. *J. Phys. C* **10**, 3107–3114 (1977)
- P. Novak, *Calculation of Spin-Orbit Coupling*, 1997. http://www.wien2k.a/reg_user/textbooks/novak_lecture_on_spinorbit.ps. Accessed 28 Jan 2015
- P.E. Blöchl, O. Jepsen, O.K. Andersen, *Phys. Rev. B* **49**, 16223–16233 (1994)
- C. Ambrosch-Draxl, J.O. Sofo, *Comp. Phys. Commun.* **175**, 1–14 (2006)
- F. Wooten, *Optical Properties of Solids* (Academic, New York, 1972)
- A.A. Lavrentyev, B.V. Gabrelian, T.V. Vu, P.N. Shkumat, P.M. Fochuk, O.V. Parasyuk, I.V. Kityk, I.V. Luzhnyi, O.Y. Khyzhun, M. Piasecki, *Inorg. Chem.* **55**, 10547–10557 (2016)
- C.D. Wagner, W.M. Riggs, L.E. Davis, J.F. Moulder, G.E. Muilenberg (eds.), *Handbook of X-ray Photoelectron Spectroscopy* (Perkin-Elmer Corp, Minnesota, 1979)
- D. Briggs, P.M. Seach (eds.), *Practical Surface Analysis: Vol. 1: Auger and X-Ray Photoelectron Spectroscopy*, 2nd edn. (Wiley, Chichester, 1990)
- S.I. Levkovets, O.Y. Khyzhun, G.L. Myronchuk, P.M. Fochuk, M. Piasecki, I.V. Kityk, A.O. Fedorchuk, V.I. Levkovets, L.V. Piskach, O.V. Parasyuk, *J. Electron Spectrosc. Relat. Phenom.* **218**, 13–20 (2017)
- O.Y. Khyzhun, O.V. Parasyuk, A.O. Fedorchuk, *Adv. Alloys Comp.* **1**, 15–29 (2014)
- B.V. Gabrelian, A.A. Lavrentyev, T.V. Vu, O.V. Parasyuk, O.Y. Khyzhun, *Opt. Mater.* **75**, 538–546 (2018)
- A.H. MacDonald, W.E. Pickett, D.D. Koelling, *J. Phys. C* **13**, 2675–2683 (1980)
- J. Kuneš, P. Novák, M. Diviš, P.M. Oppeneer, *Phys. Rev. B* **63**, 205111 (2001)
- J. Kuneš, P. Novák, R. Schmid, P. Blaha, K. Schwarz, *Phys. Rev. B* **64**, 153102 (2001)
- S. Hüfner, *Photoelectron Spectroscopy: Principles and Applications*, 3rd edn. (Springer-Verlag, Berlin/Heidelberg, 2003)
- J.C. Riviere, S. Myhra (eds.), *Handbook of Surface and Interface Analysis: Methods for Problems Solving*, 2nd edn. (CRC Press, Boca Raton/London/New York, 2009)
- O.Y. Khyzhun, T. Strunskus, W. Grünert, C. Wöll, *J. Electron Spectrosc. Relat. Phenom.* **149**, 45–50 (2005)
- O.Y. Khyzhun, T. Strunskus, Y.M. Solonin, *J. Alloys Compd.* **366**, 54–60 (2004)
- A. Meisel, G. Leonhardt, R. Szargan, *X-Ray Spectra and Chemical Binding* (Springer-Verlag, Berlin/Heidelberg, 1989)
- G. Zschornack, *Handbook of X-Ray Data* (Springer-Verlag, Berlin/Heidelberg/New York, 2007)